ACS APPLIED MATERIALS & INTERFACES

Research Article

www.acsami.org

Cocktails of Paste Coatings for Performance Enhancement of $CuInGaS_2$ Thin-Film Solar Cells

Hee Sang An,[†,‡] Yunae Cho,[§] Se Jin Park,[†] Hyo Sang Jeon,[†] Yun Jeong Hwang,[†] Dong-Wook Kim,*[,§] and Byoung Koun Min*[,†,‡]

[†]Clean Energy Research Center, Korea Institute of Science and Technology, 39-1 Hawolgok-dong, Seongbuk-gu, Seoul 136-791, Republic of Korea

[‡]Green School, Korea University, Anam-dong, Seongbuk-gu, Seoul 136-713, Republic of Korea

[§]Department of Physics, Ewha Womans University, 52, Ewhayeodae-gil, Seodaemun-gu, Seoul 120-750, Republic of Korea

Supporting Information

ABSTRACT: To fabricate low-cost and printable wide-bandgap $CuIn_xGa_{1-x}S_2$ (CIGS) thin-film solar cells, a method based on a precursor solution was developed. In particular, under this method, multiple coatings with two pastes with different properties (e.g., viscosity) because of the different binder materials added were applied. Paste A could form a thin, dense layer enabling a high-efficiency solar cell but required several coating and drying cycles for the desired film thickness. On the other hand, paste B could easily form one-micrometer-thick films by means of a one-time spin-coating process but the porous microstructure limited the solar cell performance. Three different configurations of the CIGS films (A + B, B + A, and A + B + A) were realized by multiple coatings with the two pastes to find the optimal stacking configuration for a combination of the advantages of each paste. Solar cell devices using these films showed a notable difference in their photovoltaic characteristics. The bottom dense layer increased the minority carrier diffusion length and enhanced the short-circuit current. The top dense layer could suppress interface recombination but exhibited a low optical absorption, thereby decreasing the photocurrent. As a result, the A + B configuration could be suggested as a desirable simple stacking structure. The solar cell with A + B coating showed a highly improved efficiency (4.66%) compared to the cell with a film prepared by paste B only (2.90%), achieved by simple insertion of a single thin (200 nm), dense layer between the Mo back contact and a thick porous CIGS layer.

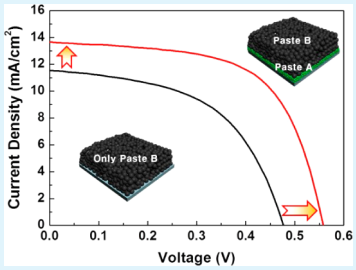

KEYWORDS: *chalcopyrite, solar cells, solution process, sulfurization, paste coating*

1. INTRODUCTION

$CuIn_xGa_{1-x}S_ySe_{2-y}$ (CIGSSe) thin-film solar cells are considered to be among the most promising alternatives to crystalline silicon solar cells due to their potential in efficiency, cost, and durability.[1,2] To fabricate CIGSSe thin-film solar cells more efficiently, ink- or paste-based coating methods for CIGSSe absorber films have been intensively developed.[3−8] In general, the preparation of solution-based CIGSSe thin films is conducted by using (1) ink (or paste), followed by (2) a coating process and (3) a heat treatment.[9−11] Depending on the specific method, there are a few differences in steps (2) and (3) because general printing methods (e.g., spin coating or doctor blading) and a heat treatment (e.g., selenization or sulfurization) are commonly used. On the other hand, the properties of the ink or paste can differ greatly among the methods devised thus far; hence, solar cells fabricated by these methods show a wide range of power conversion efficiency levels, ranging from less than 1 to more than 15%.[12,13] For example, a CIGSSe film produced from nanocrystalline ink showed a solar cell efficiency value of approximately 0.2%,[14] while a similar CIGSSe film from a hydrazine-based solution containing binary compound precursors, such as Cu_2S, In_2Se_3, or Ga_2Se_3 achieved a solar cell efficiency of 15.2%,[5] implying that the properties of the ink or the paste are crucial in determining the quality of CIGSSe thin films and therefore the solar cell performance level.

Recently, we have developed a precursor-solution-based method for the preparation of wide-bandgap $CuInGaS_2$ (CIGS) thin films in which most of the procedures, including the paste preparation and film deposition steps, were conducted under ambient air conditions, as opposed to restricted conditions (i.e., in a glove box).[15] Furthermore, an alcohol, such as ethanol or methanol, was used as solvent for the paste solution that is much less harmful and easier to handle compared to toxic solvents, such as hydrazine. However, we have also found that the properties of the CIGS films are strongly influenced by the properties of the precursor solution paste, even if identical coating and heat treatment processes are applied.[15−22]

For example, a paste prepared by Cu, In, and Ga nitrate precursors in methanol with polyvinyl acetate (PVA) as organic binder resulted in a densely packed CIGS film, but it required multiple coating and drying cycles to achieve a proper film

Received: September 24, 2013
Accepted: December 20, 2013
Published: December 20, 2013

thickness. On the other hand, another paste prepared using the same Cu, In, and Ga nitrate precursors dissolved in ethanol with ethyl cellulose as organic binder revealed a high degree of porosity, but it could be easily applied to realize the desired film thickness (~1.2 μm) by spin coating or by the doctor blade coating method.

On the basis of our previous studies it can be expected that a suitable combination of the beneficial properties of each paste will lead to a more efficient fabrication of CIGS thin films (fewer coating and drying cycles) and an improved solar cell performance. In this study, to realize this objective, we introduced a novel synthesis method of CIGS films by multiple coatings with two pastes with different properties: one for a dense and thin layer and the other for a porous and thick layer. Three different types of stacked CIGS films were prepared using this method, and their morphological and photovoltaic characteristics were investigated.

2. EXPERIMENTAL SECTION

2.1. Preparation of the Pastes. *Paste A:* A precursor mixture solution was prepared by dissolving appropriate amounts of $Cu(NO_3)_2{\cdot}xH_2O$ (99.999%, Alfa Aesar, 1.0 g), $In(NO_3)_3{\cdot}xH_2O$ (99.99%, Alfa Aesar, 1.12 g), and $Ga(NO_3)_3{\cdot}xH_2O$ (99.999%, Alfa Aesar, 0.41 g) in methanol (7.0 mL), followed by the adding of a methanol solution (7.0 mL) with poly-vinyl acetate (PVA) (Aldrich, 1.0 g). After the mixture solution was stirred with a magnetic bar for 30 min, a paste suitable for spin-coating was prepared.

Paste B: A precursor mixture solution was prepared by dissolving appropriate amounts of $Cu(NO_3)_2{\cdot}xH_2O$ (99.999%, Alfa Aesar, 1.0 g), $In(NO_3)_3{\cdot}xH_2O$ (99.99%, Alfa Aesar, 1.12 g), and $Ga(NO_3)_3{\cdot}xH_2O$ (99.999%, Alfa Aesar, 0.41 g) in anhydrous ethanol (80 mL), followed by an addition of ethanol solution (20 mL) with terpineol (Fluka, 13.7 g) and ethyl cellulose (Aldrich, 0.75 g). After the mixture solution was condensed at 40 °C under reduced pressure, a viscous paste with rheological properties suitable for spin-coating was prepared.

2.2. Synthesis of the CIGS Films. CIGS thin films were synthesized by paste coating and subsequent two step heat treatment of oxidation and sulfurization. The paste was spin-casted onto a Mo-coated glass substrate, and the film was then dried at 150 and 300 °C for first layer and second layer using a hot plate for 3 min, respectively. The dried film was annealed at 350 °C for 1 h under ambient conditions in a furnace, resulting in a mixed oxide film of Cu, In, and Ga. The CIGS alloy film was then formed by reacting this oxidized film with dilute H_2S gas ($H_2S(1\%)/N_2$) at an elevated temperature (500 °C) for 30 min.

2.3. Fabrication of the Solar Cell Device. The solar cell devices were fabricated according to the conventional configuration (Mo/CIGS/CdS/*i*-ZnO/*n*-ZnO/Ni/Al). In our process, a 60 nm thick CdS buffer layer was deposited on CIGS film by chemical bath deposition (CBD), and *i*-ZnO (50 nm)/Al doped *n*-ZnO (500 nm) layers were deposited by radio-frequency (RF) magnetron sputtering on the CdS layer. A Ni (50 nm) and Al (500 nm) grid thick was deposited as a current collector by thermal evaporation. The active area of the completed cells was 0.44 cm^2.

2.4. Characterization. Structural characterization of the films was performed using a scanning electron microscope (SEM, FEI, Nova-Nano200) with a 10 kV acceleration voltage and an X-ray diffraction (XRD, Shimadzu, XRD-6000) with Cu Kα radiation (λ = 0.15406 nm). Composition analysis was carried out with an electron probe microanalyzer (EPMA, JEOL Ltd., Tokyo, Japan). Viscosities of the pastes were measured at 25 °C using a cone−plate type viscometer (TVE-22LT, Toki Sangyo Co. Ltd). Optical properties were measured by a diffuse reflectance UV−vis spectrophotometer (Cary 5000, Varian). Device performances were characterized using a class AAA solar simulator (Wacom, Saitama, Japan) and an incident photon conversion efficiency (IPCE) measurement unit (Soma Optics, Tokyo, Japan). DC transport characteristics were measured using a Keithley 4200 semiconductor characterization system in a cryogenic vacuum probe station (Janis Co., ST-500) over the temperature range of 100−300 K.

3. RESULTS AND DISCUSSION

As briefly described earlier, two different paste solutions were prepared and applied to make wide-bandgap CIGS thin films. Paste A appeared in blue with a viscosity of 15 ± 5 cP at 25 °C. On the other hand, paste B revealed a similar blue color, but its viscosity was measured to be 4000 ± 100 cP at 25 °C. In fact, this viscosity difference resulted from amount used, as well as intrinsic property of the binder materials. Because of the relatively high viscosity of paste B, the desired film thickness (~1.2 μm) could be easily achieved by a one-time spin coating. However, the resulting CIGS films revealed a high degree of porosity, which led to relatively low solar cell efficiencies (<3%) of devices created by using these films (see Supporting Information Figure S1).

Notably, very different from paste B, paste A required multiple coating and drying cycles to achieve a proper film thickness. For example, a ~1.2-μm-thick film could be achieved by six cycles of coating and drying, which would lead to a low throughput during large scale production. Interestingly, however, the CIGS film produced from this paste showed a densely packed film morphology concomitant with the generation of much higher power conversion performance levels (8.3%) as compared to the films fabricated from paste B.[15]

In order to combine the beneficial properties of two pastes, we introduced cocktails of paste coatings using both paste A and B, as schematically described in Figure 1. The notation A + B indicates the film configuration, in which a thin film (~0.2 μm) was initially attained by a one-time coating with paste A, followed by an additional coating with paste B to form a thick layer (~1 μm) on top of the dense film created by paste A. Meanwhile, the notation of B+A indicates a film arrangement in which a porous and thick layer (~1 μm) by paste B was prepared prior to the dense and thin layer (~0.2 μm) consisting of paste A. A sandwich configuration A + B + A was also prepared, in which both top (~0.2 μm) and bottom

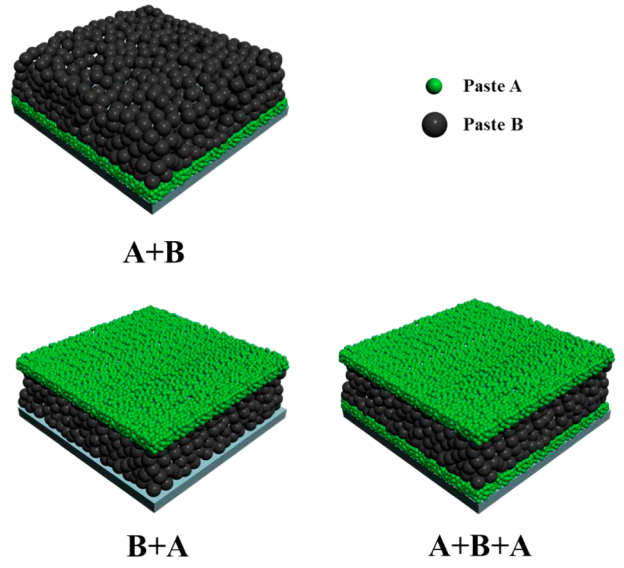

Figure 1. Schematics of CIGS film configurations prepared by the multiple-paste-coating method.

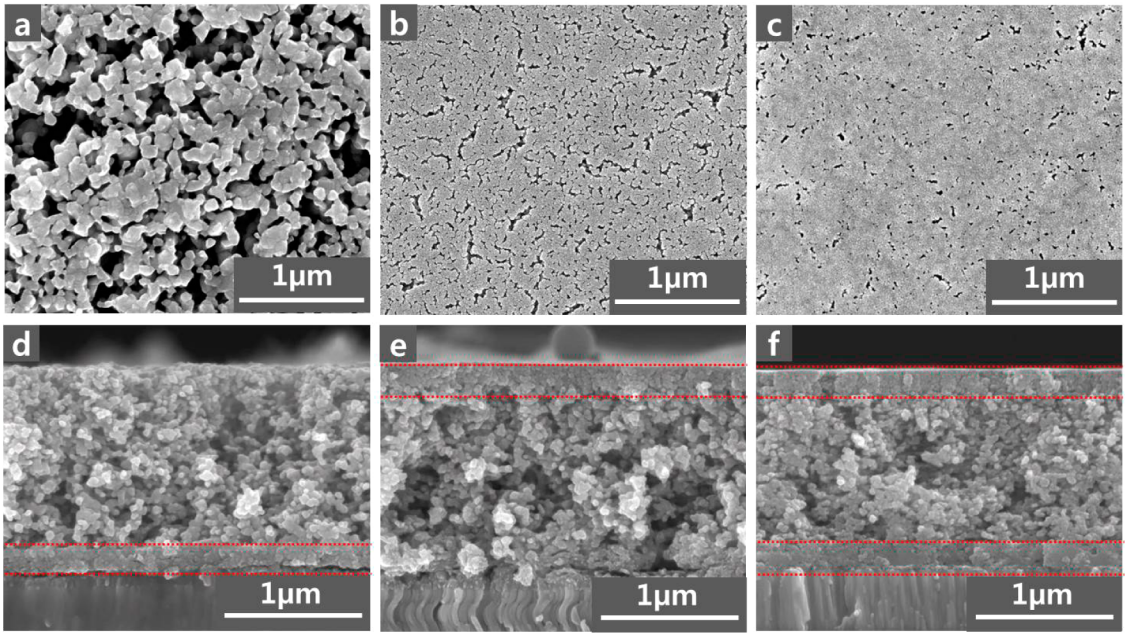

Figure 2. Top view (a, b, and c) and cross-sectional (d, e, and f) SEM images of three different CIGS film arrangements: (a and d) A + B, (b and e) B + A, and (c and f) A + B + A. Red dashed lines indicate the demarcation between the individual layers prepared by the two different pastes A and B.

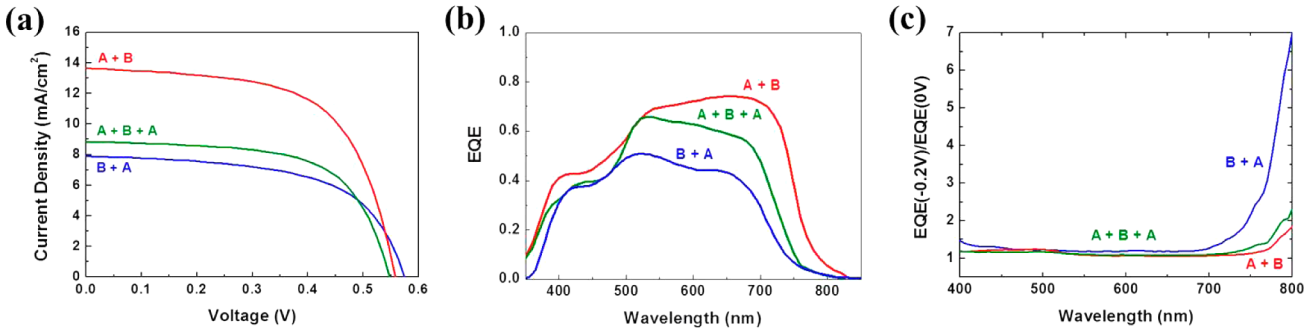

Figure 3. (a) *J*–*V* characteristics of representative CIGS solar cell devices with different layers of films under 1 sun illumination, (b) external quantum efficiency (EQE) of the three types of CIGS solar cells at zero bias, (c) EQE ratios at −0.2 and 0 V biases of the CIGS solar cells.

thin layers (~0.2 μm) were fabricated by paste A and a middle thicker layer (~0.8 μm) by paste B. The overall film thicknesses were adjusted so that they were virtually identical (~1.2 μm) by controlling the spinning speed of the spin coater to avoid any ambiguity caused by a varying film thickness.

Figure 2 shows the morphologies of the CIGS films obtained by the multiple coating with pastes A and B and subsequent oxidation and sulfurization steps. For the fabrication of the CIGS film with A + B configuration, paste A was spin-casted onto a Mo-coated glass substrate. The film was then dried at 150 °C under ambient conditions using a hot plate. On top of the dried film, paste B was spin-casted and dried at 300 °C, again using a hot plate. The dried films of A + B configuration were annealed at 350 °C for 1 h under ambient conditions in a furnace, resulting in a mixed oxide film of Cu, In, and Ga. Because of this this heat treatment the amount of residual carbon was found to be dramatically reduced (<5 wt %) based on an electron probe microanalyzer (EPMA) analysis. The CIGS alloy film was then synthesized by reacting this film composite with dilute H_2S gas ($H_2S(1\%)/N_2$) at an elevated temperature (500 °C). The surface morphology of the highly porous CIGS film formed only by paste B was observed in the corresponding top-view scanning electron microscopy (SEM) image (Figure 2a). In contrast, the densely packed film created by paste A at the bottom of the film configuration was more clearly confirmed by the cross-sectional SEM image shown in Figure 2d, revealing an apparent line of demarcation due to the different compactness of the layers formed by paste A and B (as denoted by the dashed lines).

The reverse film configuration B + A (Figures 2b and e) was constructed by a similar coating method except for the coating order. In this case, paste B was initially coated, followed by drying and subsequent coating with paste A. After a sulfurization step, the surface morphology was found to be significantly different from that of the A + B film, as shown in Figure 2b. A dense surface was noted due to the second coating with paste A. Furthermore, a sandwich configuration A + B+ A (Figures 2c and f) was also constructed by the successive coating of paste A, paste B, and again paste A with drying between each coating step. After sulfurization, a surface morphology similar to that of Figure 2b was observed because a dense layer formed by paste A was prepared on top of the film composite (Figure 2c). Notably, the X-ray diffraction (XRD) patterns of the films arranged in the three different

dx.doi.org/10.1021/am404164b | *ACS Appl. Mater. Interfaces* 2014, 6, 888−893

configurations did not differ, thus indicating that the crystal structure is not influenced by the film configuration (see Supporting Information Figure S2).

To investigate the effects of the multiple-paste-coating method on the solar cell performance, solar cell devices were constructed based on a substrate-type configuration (Al/Ni/ZnO:Al/i-ZnO/CdS/CIGS/Mo coated glass). General deposition procedures were applied for a CdS buffer layer (chemical bath deposition) and a ZnO window layer (sputtering deposition). Current density−voltage (J−V) measurements of the solar cell devices showed very different features, depending on the absorber film configurations (Figure 3a and Table 1).

Table 1. Average Performance Values of Eight CIGS Thin-Film Solar Cell Devices with Different Absorber Film Configurations

sample	V_{oc} (mV)	J_{sc} (mA/cm^2)	FF (%)	η (%)
A + B	537	14.4	60.2	4.66
B + A	572	8.13	58.1	2.71
A+B+A	523	9.87	57.5	2.94

The solar cell device with B + A film configuration showed the highest open-circuit voltage (V_{oc}) but the lowest power conversion efficiency (average of 2.71% and best value of 2.90%) due to the low short-circuit current (J_{sc}). Compared to the solar cell with a film prepared by paste B only (see supporting information Figure S1), the increase of V_{oc} is noticeable. However, the decrease of J_{sc} resulted in no improvement of the overall solar cell efficiency. On the other hand, when the bottom layer of the CIGS film (on top of Mo) was synthesized by paste A (i.e., A + B and A + B + A), J_{sc} increased while V_{oc} decreased, compared to the B + A configuration. The highest power conversion efficiency (average of 4.66% and best value of 5.19%) was obtained by the solar cell device with the CIGS film configuration A + B. Based on the J−V characteristics of the solar cell devices with the three different absorber film configurations, it can be inferred that the dense layer formed by paste A at the bottom (at the interface with the Mo back-contact electrode) helps to increase J_{sc}, whereas the same layer on top (interface with CdS buffer layer) reduces J_{sc}.

For a better understanding of the solar cell performance in dependence of the absorber film on figuration, the wavelength- and bias-dependent external quantum efficiencies (EQE) were investigated. Figure 3b shows that the EQE of the CIGS solar cell clearly depends on the stacking configuration of the dense and porous layers. The solar cell with A + B film arrangement exhibited the best carrier collection efficiency at long wavelengths among the three investigated kinds of cells. In contrast, a significant drop in the EQE data of the cell with B + A configuration is remarkable, compared with the other types of cells.

EQE data under reverse bias can further clarify the origin of the poor spectral response of the solar cell device with B + A configuration.[5,6,24] The reverse bias can enlarge the depletion width in the absorber film, and thereby, increased EQE in case the electrical recombination loss in the cell is significant. As shown in Figure 3c, the EQE(-0.2 V)/EQE(0 V) ratios of the CIGS solar cells with A + B and A + B + A configuration did not vary greatly. The ratio of the cell with B + A configuration, however, increased considerably at long wavelengths (> 700 nm). This indicates that the poor EQE characteristics of the B + A film are mainly caused by the electrical loss. It should be also noted that the dense bottom layer can enhance the spectral response because of the long minority carrier diffusion length.[24] Therefore, the difference in the EQE data of the cells with A + B and A + B + A layer arrangement should be attributed to optical rather than to electrical loss, since the reverse bias could not vary the EQE results. In fact, the samples with a dense top layer (B + A and A + B + A) exhibited a somewhat higher optical reflectance than that with the porous top layer (A + B) (see Supporting Information Figure S3). It seems that the relatively large grains and pores in the porous layers can scatter incident light efficiently and thereby lower the optical reflectance. Such an optical gain in the porous top layer enabled an increase of the photocurrent of the solar cell.

The dark J−V characteristics of the CIGS solar cells follow the well-known diode equation $J_{diode} = J_0[\exp(qV/Ak_BT)-1]$ where J_0, A, q, k_B, and T are the saturation current density, the diode ideality factor, the electron charge, the Boltzmann constant, and temperature, respectively.[25] J_0 shows an activation behavior with the characteristic energy E_a: $J_0 = J_{00}\exp(-E_a/Ak_BT)$. J_{00} is the reference current density which is only weakly temperature-dependent.[25] Thus, $A\ln(J_0)$ shows a linear dependence on $1/T$, as shown in Figure 4.

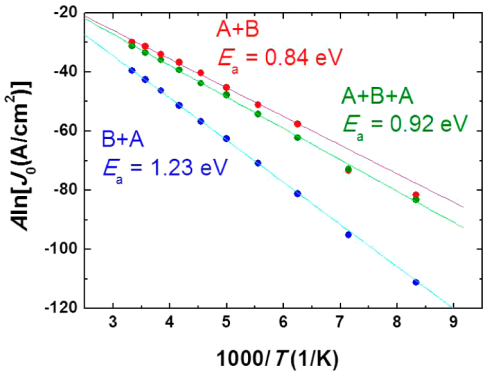

Figure 4. Plots of $A\ln J_0$ as a function of the inverse temperature for the CIGS solar cells (A = ideality factor, J_0 = saturation current density).

The E_a values can be extracted from the slopes of the linear curves and amount to 0.84, 1.23, and 0.92 eV for A + B, B + A, and A + B + A, respectively. These E_a values are smaller than the bandgap energy of CIGS, 1.62−1.65 eV, as estimated from the reflectance spectra of the CIGS films (see Supporting Information Figure S3). This indicates that the major recombination process occurs at the interface rather than in the bulk of the CIGS films.[24,25] The diode ideality factor A of the CIGS solar cells showed a significant increase as temperature decreased and was as large as 4−6 at 100 K (see Supporting Information Figure S4). Such a temperature dependence of A indicates that tunneling-enhanced recombination at the interface is the dominating process in all of our CIGS solar cells.[25] The E_a values of the cells with dense top layer (B + A and A + B + A) were larger than that of the cell with A + B configuration. This suggests that the dense top layer helped to reduce the defect concentration near the CdS/CIGS junction and suppresses trap-mediated recombination at the interface. A porous top layer is not supposed to form a well-defined p−n junction with the CdS buffer layer and may even induce Cd diffusion from the CdS buffer into the CIGS layer.[23] Such poor interfaces can cause the creation of recombination

dx.doi.org/10.1021/am404164b | ACS Appl. Mater. Interfaces 2014, 6, 888−893

sites, as well as leakage currents. Indeed, a solar cell with a film prepared using only paste B (very porous throughout the film) revealed a low V_{oc} and low efficiency (see Supporting Information Figure S1).

The effect of the dense layer on the performance of the CIGS solar cell is not straightforward, as discussed above. Most of all, its influence strongly depended on the location within the cell (top, bottom, or top-and-bottom). To gain more insight into this issue, the microstructure of the absorber film was more carefully investigated. Figure 5 shows SEM images of each layer

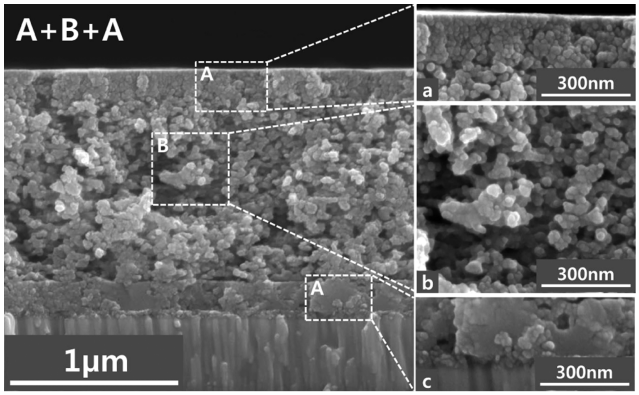

Figure 5. Cross-sectional SEM image of the CIGS thin film with A + B + A configuration (left) and the magnified images of each layer: (a) top layer by paste A, (b) middle layer by paste B, and (c) bottom layer by paste A.

of the CIGS film with A + B + A configuration at higher resolution. The middle part of the film consisting of paste B shows a highly porous morphology composed of grains with an average diameter of 34 nm. Notably, the top and bottom layers reveal distinctively different morphologies, even though they were made by the same material (paste A). The top layer shows a very densely packed film composed of small grains with an average diameter of 20 nm. Instead, the bottom layer consists of very large grains, as seen in Figure 5c. It should be noted that the morphology of this bottom layer is much closer to that of a typical film synthesized by only paste A (see Supporting Information Figure S5), which has shown a much higher performance in solar cell applications.[15] The stacking sequence influenced the microstructures of the CIGS layers even in case they were prepared by the same paste. Obviously, the underlying layers should influence the structural properties of thin films grown on top of them. As shown in Figure 5a, the top dense layer was composed of small-sized grains, and hence, carriers will undergo scattering while crossing the grain boundaries.[26] Thus, such high-density grain boundaries may limit the collection of photocarriers. Such a grain boundary effect may provide additional clues to explain why the presence of a dense top layer reduces J_{sc} despite the beneficial effect of a suppression of recombination at the CdS/CIGS interface (Figure 4). Different from the effect of an upper dense layer, a bottom dense layer consists of highly crystalline large grains, thus leading to a much better charge transport, as evident from the EQE data (Figures 3b and 3c).

4. CONCLUSIONS

In brief, in this study, we introduced a novel synthesis method of CIGS films by multiple coatings with two pastes with different properties: one for a dense and thin layer and the other for a porous and thick layer. We compared the photovoltaic characteristics of solar cells with several types of stacked films and suggested a more efficient (requiring fewer coating and drying cycles) fabrication method of CIGS thin films with improved performance. We found that the stacking configuration of the CIGS layers significantly influenced the performance of the solar cells that is closely related to the microstructure of the layers. The dense CIGS layer on the Mo back contact helped to increase the minority carrier diffusion length and raised the photocurrent. The top dense layer could suppress interface recombination but its low optical absorption limited the maximum achievable photocurrent. The dense top layer composed of small grains seems to induce an additional reduction of the photocurrent due to grain boundary effects. The CIGS solar cell consisting of a dense bottom layer and a porous top layer resulted in an efficiency of 4.66%, much higher than the efficiency (2.90%) of a cell consisting of a porous layer only.

■ ASSOCIATED CONTENT

Supporting Information

SEM and $J-V$ data of CIGS films, XRD and reflectance data of the CIGS thin films, and the diode ideality factor of the CIGS solar cells. This material is available free of charge via the Internet at http://pubs.acs.org/.

■ AUTHOR INFORMATION

Corresponding Authors

*Tel.: +82 2 3277 6668. Fax: +82 2 3277 2372. E-mail: dwkim@ewha.ac.kr.

*Tel.: +82 2 958 5853. Fax: +82 2 958 5809. E-mail: bkmin@kist.re.kr.

Notes

The authors declare no competing financial interest.

■ ACKNOWLEDGMENTS

This work was supported by the University-Institute cooperation program of the National Research Foundation of Korea Grant funded by the Korean Government (MSIP). Also, the authors would like to thank the program of Converging Research Center Program through the National Research Foundation of Korea Grant (2011-K000580) and (NRF-2009-C1AAA001-0092935), funded by the Korean Government(MSIP), and the program of Korea Institute of Science and Technology (KIST).

■ REFERENCES

(1) Hegedus, S. *Prog. Photovoltaics* **2006**, *14*, 393−411.
(2) Jackson, P.; Hariskos, D.; Lotter, E.; Paetel, S.; Wuerz, R.; Menner, R.; Wischmann, W.; Powalla, M. *Prog. Photovoltaics* **2011**, *19*, 894−897.
(3) Kaelin, M.; Rudmann, D.; Tiwari, A. N. *Sol. Energy* **2004**, *77*, 749−756.
(4) Kapur, V. K.; Bansal, A.; Le, P.; Asensio, O. I. *Thin Solid Films* **2003**, *431−432*, 53−57.
(5) Todorov, T. K.; Gunawan, O.; Gokmen, T.; Mitzi, D. B. *Prog. Photovoltaics* **2012**, *21*, 82−87.
(6) Guo, Q.; Ford, G. M.; Agrawal, R.; Hillhouse, H. W. *Prog. Photovoltaics* **2012**, *21*, 64−71.
(7) Stolle, C. J.; Harvey, T. B.; Korgel, B. A. *Curr. Opin. Chem. Eng.* **2013**, *2*, 160−167.
(8) Wang, G.; Wang, S.; Cui, Y.; Pan, D. *Chem. Mater.* **2012**, *24*, 3993−3997.

(9) Habas, S. E.; Platt, H. A. S.; van Hest, M.; Ginley, D. S. *Chem. Rev.* **2010**, *110*, 6571−6594.
(10) Hibberd, C. J.; Chassaing, E.; Liu, W.; Mitzi, D. B.; Lincot, D.; Tiwari, A. N. *Prog. Photovoltaics* **2010**, *18*, 434−452.
(11) Todorov, T.; Mitzi, D. B. *Eur. J. Inorg. Chem.* **2010**, *2010*, 17−28.
(12) Akhavan, V. A.; Goodfellow, B. W.; Panthani, M. G.; Steinhagen, C.; Harvey, T. B.; Stolle, C. J.; Korgel, B. A. *J. Solid State Chem.* **2012**, *189*, 2−12.
(13) Bob, B.; Lei, B.; Chung, C.-H.; Yang, W.; Hsu, W.-C.; Duan, H.-S.; Hou, W. W.-J.; Li, S.-H.; Yang, Y. *Adv. Energy Mater.* **2012**, *2*, 504−522.
(14) Panthani, M. G.; Akhavan, V.; Goodfellow, B.; Schmidtke, J. P.; Dunn, L.; Dodabalapur, A.; Barbara, P. F.; Korgel, B. A. *J. Am. Chem. Soc.* **2008**, *130*, 16770−16777.
(15) Park, S. J.; Cho, J. W.; Lee, J. K.; Shin, K.; Kim, J.-H.; Min, B. K. *Prog. Photovoltaics* **2014**, *22*, 122−128.
(16) Wang, W.; Su, Y. W.; Chang, C. H. *Sol. Energy Mater. Sol. Cells* **2011**, *95*, 2616−2620.
(17) Uhl, A. R.; Romanyuk, Y. E.; Tiwari, A. N. *Thin Solid Films* **2011**, *519*, 7259−7263.
(18) Ahn, S.; Son, T. H.; Cho, A.; Gwak, J.; Yun, J. H.; Shin, K.; Ahn, S. K.; Park, S. H.; Yoon, K. *ChemSusChem* **2012**, *5*, 1773−1777.
(19) Kim, K.; Eo, Y. J.; Cho, A.; Gwak, J.; Yun, J. H.; Shin, K.; Ahn, S. K.; Park, S. H.; Yoon, K.; Ahn, S. *J. Mater. Chem.* **2012**, *22*, 8444−8448.
(20) Lim, Y. S.; Jeong, J.; Kim, J. Y.; Ko, M. J.; Kim, H.; Kim, B.; Jeong, U.; Lee, D.-K. *J. Phys. Chem. C* **2013**, *117*, 11930−11940.
(21) Uhl, A. R.; Fella, C.; Chirilă, A.; Kaelin, M. R.; Karvonen, L.; Weidenkaff, A.; Borca, C. N.; Grolimund, D.; Romanyuk, Y. E.; Tiwari, A. N. *Prog. Photovoltaics* **2012**, *20*, 526−533.
(22) Lee, E.; Park, S. J.; Cho, J. W.; Gwak, J.; Oh, M. K.; Min, B. K. *Sol. Energy Mater. Sol. Cells* **2011**, *95*, 2928−2932.
(23) Jeong, S.; Lee, B.-S.; Ahn, S.; Yoon, K.; Seo, Y.-H.; Choi, Y.; Ryu, B.-H. *Energy Environ. Sci.* **2012**, *5*, 7539−7542.
(24) Barkhouse, D. A. R.; Gunawan, O.; Gokmen, T.; Todorov, T. K.; Mitzi, D. B. *Prog. Photovoltaics* **2012**, *20*, 6−11.
(25) Scheer, R.; Schock, H.W. In *Chalcogenide Photovoltaics*; Wiley-VCH Verlag GmbH & Co. KGaA: Weinheim, Germany, 2011; p 111.
(26) Virtuani, A.; Lotter, E.; Powalla, M.; Rau, U.; Werner, J. H.; Acciarri, M. *J. Appl. Phys.* **2006**, *99*, 014906.